



CHORUS

This is the accepted manuscript made available via CHORUS. The article has been published as:

Phonon-mediated superconductivity in electron-doped single-layer MoS₂: A first-principles prediction

Yizhi Ge and Amy Y. Liu

Phys. Rev. B **87**, 241408 — Published 24 June 2013

DOI: [10.1103/PhysRevB.87.241408](https://doi.org/10.1103/PhysRevB.87.241408)

Phonon-mediated superconductivity in electron-doped single-layer MoS₂

Yizhi Ge and Amy Y. Liu

Department of Physics, Georgetown University, Washington, DC 20057

The electron-phonon interaction in electron-doped single-layer MoS₂ is investigated using first-principles calculations. The electron-phonon coupling is found to be very weak at low doping levels. It then grows rapidly to a maximum of about $\lambda \approx 1.7$, after which it begins to decrease with additional doping. The superconducting transition temperature is expected to follow the same trends. This behavior is attributed to the growth and shrinkage of Fermi sheets with different orbital character. These results, which are similar to the experimentally observed superconducting dome in gate-tuned MoS₂ thin flakes, reveal that having the right combination of electronic states at the Fermi level is crucial for optimizing the electron-phonon interaction in this material. By appropriately tuning the band structure, it may be possible to further enhance the superconducting properties of this material.

PACS numbers:

Molybdenum disulfide (MoS₂) is a transition-metal dichalcogenide that consists of S-Mo-S trilayers that are weakly bound to each other.¹ A semiconductor with an indirect gap of about 1.2 eV,² bulk MoS₂ has been of interest for its tribological,³ catalytic,^{4,5} and photovoltaic^{6,7} properties. In addition, bulk MoS₂ is easily metallized through insertion of alkali or alkaline earth metals into the Van der Waals gap between trilayers, and many of these intercalated compounds become superconducting when cooled.⁸ K_xMoS₂, for example, has a maximum superconducting transition temperature of about 7 K when $x \approx 0.4$.⁹ This is similar to the transition temperature in NbSe₂, which has the highest superconducting T_c among metallic transition-metal dichalcogenides.

Recently, it has been demonstrated that single-layer MoS₂ can be produced by mechanical and chemical exfoliation techniques¹⁰ and by direct growth methods.¹¹ Unlike the bulk material, single-layer MoS₂ (consisting of one S-Mo-S trilayer) has a direct band gap of 1.9 eV.^{12–14} With its reduced dimensionality and large direct band gap, single-layer MoS₂ has quickly attracted attention for use in nanoscale electronic and photonic devices. Ultrathin MoS₂ has been successfully fabricated into field-effect transistors (FET) with high on-off ratios,¹⁵ and it is being investigated for its chemical sensing¹⁶ and photovoltaic properties.¹⁷

Raman spectroscopy of field-effect-doped single-layer MoS₂ has found that the Raman-active A_{1g} mode softens and broadens significantly with electron doping.¹⁸ This is attributed to strong coupling of the mode to electronic states at the bottom of the conduction band. This indication of a strong electron-phonon interaction in the monolayer, combined with the existence of superconducting phases in intercalated bulk compounds, raises the question of whether phonon-mediated superconductivity can be induced in single-layer MoS₂. If so, the material could be useful for novel nanoscale devices that integrate electronic, optical, and superconducting components.

Recent experiments on liquid-gated thin-flake MoS₂ transistors have discovered a dome-shaped superconducting region in the temperature versus doping plane of the

phase diagram.¹⁹ While the samples in these experiments are not atomically thin, it is argued that the carriers are concentrated in the top layer. For carrier densities below $n_{2d} = 6 \times 10^{14} \text{ cm}^{-2}$, corresponding to a monolayer doping concentration of $x \approx 0.05$ electrons per formula unit, no superconducting transition is observed (down to 2 K). Above this doping concentration, the superconducting T_c rises sharply, reaching a maximum of about 11 K near $x = 0.1$ electrons/f.u. Then the superconducting phase line turns over. While it was not possible in these experiments to achieve higher doping levels comparable to the intercalated bulk compounds, it was suggested that the data for the alkali-intercalated bulk superconductors might connect smoothly to the superconducting dome mapped out for the liquid-gated thin flakes.¹⁹

In this work we use density-functional-theory (DFT) calculations to investigate the electronic and vibrational properties of electron-doped single-layer MoS₂ to explore the possibility of phonon-mediated superconductivity in a true monolayer. The electron-phonon coupling strength is studied as a function of doping. We find the onset of superconductivity at a low but non-zero doping concentration, as well as a subsequent turnaround in T_c , both of which can be attributed to changes in the number and size of Fermi sheets as the carrier concentration is varied. These results suggest that further enhancements in T_c might be possible via appropriate tuning of the band structure.

Calculations were carried out using the Quantum Espresso package.²⁰ Ultrasoft pseudopotentials were used to describe the interaction between electrons and ionic cores,²¹ and the local density approximation was adopted for the exchange-correlation potential.²² A plane-wave basis with a 35 Ry energy cut-off was used to represent electronic wave functions. The Brillouin zone was sampled with a $24 \times 24 \times 1$ mesh of \mathbf{k} -points for calculation of the total energy and electron charge density. Phonon spectra and electron-phonon coupling constants were calculated using density-functional perturbation theory.²³ The double Fermi-surface average of electron-phonon matrix elements was done using grids

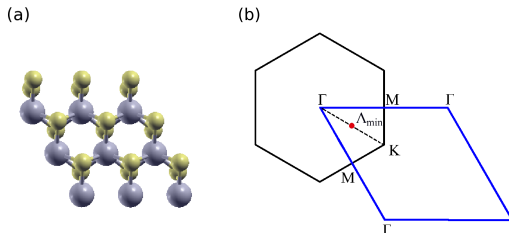


FIG. 1: (Color online) (a) Top view of the atomic structure of single-layer MoS₂. Large spheres represent Mo atoms on a triangular lattice. Small spheres represent S atoms, which lie in planes above and below the Mo plane. (b) High-symmetry points in the Brillouin zone.

of $288 \times 288 \times 1$ \mathbf{k} -points with a smearing parameter of $\sigma = 0.002$ Ry. Doping was simulated by adding electrons to the system, together with a compensating uniform positive background.

Figure 1 (a) shows the top view of the crystal structure of single-layer MoS₂. Each atomic sheet consists of a hexagonal close-packed lattice, and the sheets are stacked so that each Mo atom is coordinated by a trigonal prism of S sites. To model the single layer, we used a supercell with at least 14.5 Å of vacuum to avoid interaction between layers. The in-plane lattice constant was held fixed at the optimized value for the undoped material (3.122 Å), while the distance between Mo and S atomic planes was relaxed at each doping concentration until forces were less than 10^{-3} Ry/au. Previous DFT studies of MoS₂ have found that the choice of exchange-correlation functional affects the optimized geometry, which in turn affects how vibrational frequencies evolve in going from bulk to monolayer.²⁴ The present work considers only the monolayer and focuses on the effects of doping. While details of the electronic structure and vibrational spectrum depend on geometry and functional, the qualitative effects of doping are relatively insensitive to these choices.

Undoped single-layer MoS₂ is calculated to have a conduction-band minimum at the K point in the Brillouin zone, and a second conduction-band minimum located about halfway between Γ and K (along the Λ line), about 110 meV higher in energy. The conduction-band minimum at K has strong Mo d_{z^2} character, while states near the second minimum are derived from a combination of in-plane d orbitals on the Mo sites and out-of-plane p_z orbitals on the S sites. These results are consistent with previous DFT results.^{25–27} Both spin-orbit interactions²⁸ and many-body effects beyond DFT^{27,29,30} have been shown to have significant impact on the band structure. However, the conduction band, which is the focus of the present work, retains the same qualitative features and trends.

Figure 2 shows the conduction band along the Λ line (Γ to K) as a function of doping, along with the corresponding Fermi surfaces. At low doping concentrations,

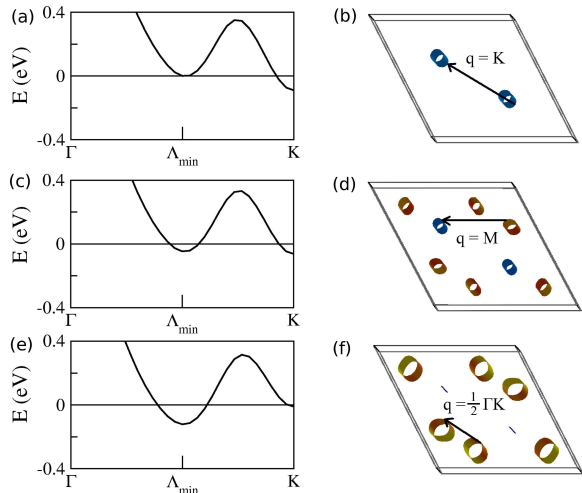


FIG. 2: (Color online) Conduction band and Fermi surface of single-layer MoS₂. Panels (a) and (b) correspond to a doping concentration of $x = 0.03$ electrons/f.u., panels (c) and (d) show results for $x = 0.10$ electrons/f.u., and panels (e) and (f) are for $x = 0.22$ electrons/f.u. Some representative phonon wave vectors that connect Fermi sheets are shown.

such as $x = 0.03$ electrons/f.u., electrons occupy states near the conduction-band minimum at K, as seen in Fig. 2(a). Figure 2(b) shows the corresponding Fermi sheets around the two K points in the Brillouin zone. With more doping, the second valley, centered at Λ_{min} , becomes occupied as well, and new Fermi sheets appear, as in Figs. 2(c) and (d), which show results for $x = 0.10$ electrons/f.u. Note that as the concentration of charge carriers increases, the energy difference between the Λ_{min} and K valleys decreases, and eventually becomes negative. At $x = 0.22$ electrons/f.u., the Λ_{min} valley lies below the K valley and there is barely a Fermi surface around the K points [Figs. 2(e) and (f)].

The relative shift in energy of the conduction band valleys with doping can be explained by considering the character of the electronic states involved. Dominated by Mo d_{z^2} character, states near the original conduction-band minimum at K are more localized than the Λ_{min} states, which project strongly onto both Mo d_{xy/x^2-y^2} and S p_z orbitals. As charge carriers are added, Coulomb repulsion pushes the more localized states near K up in energy, and leads to the eventual reversal in order of the two valleys.

The phonon spectra calculated for undoped and electron-doped single-layer MoS₂ are presented in Fig. 3. The Raman-active modes at the zone center are in reasonable agreement with experiments and prior calculations.^{18,24,31–33} As noted in Ref. 18, the A_{1g} mode, which is slightly above 400 cm^{-1} , softens considerably when doped, while the two-fold degenerate E_{2g}^1 mode below 400 cm^{-1} is relatively insensitive to doping. However, the most significant softening occurs not in the optical branches near the zone center, but rather in the highest

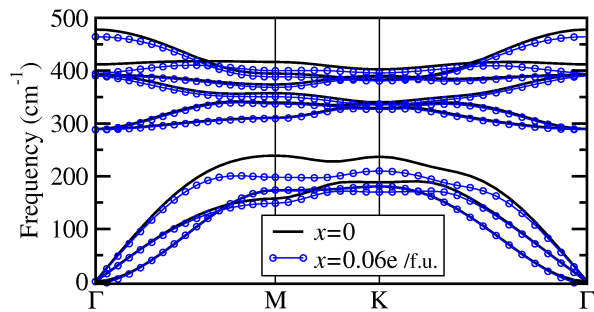


FIG. 3: Phonon dispersion curves calculated for single-layer MoS₂. Solid curves are for the undoped material, while circles show results for $x = 0.06$ electrons/f.u.

acoustic branch, particularly near the M and K points at the zone boundary. The optical A_{1g} mode involves out-of-plane displacement of the S atoms, which interact strongly with the Mo d_{z^2} states at the conduction-band minimum. When these electronic states become occupied, the phonon frequency is renormalized due to increased screening. On the other hand, the highest acoustic phonon branch involves longitudinal in-plane displacement of Mo atoms (the direction of S displacements depends on the phonon wave vector). The softening of the longitudinal acoustic branch arises from strong coupling of this mode to electrons in the Λ_{min} valley of the conduction band, as discussed below.

The Fermi surface average of the square of the electron-phonon matrix element is

$$\langle\langle |g_{\mathbf{q}\nu}|^2 \rangle\rangle = \frac{\sum_{\mathbf{k}j j'} |g_{\mathbf{k}j; \mathbf{k}+\mathbf{q}j'; \mathbf{q}\nu}|^2 \delta(\epsilon_{\mathbf{k}j}) \delta(\epsilon_{\mathbf{k}+\mathbf{q}j'})}{[N(0)]^2}, \quad (1)$$

where the Fermi level is set to zero, $N(0)$ is the density of states at the Fermi level, and $g_{\mathbf{k}j; \mathbf{k}+\mathbf{q}j'; \mathbf{q}\nu}$ is the matrix element for scattering an electron from state $\mathbf{k}j$ (j is a band index) to state $\mathbf{k}+\mathbf{q}j'$ by a phonon with wave vector \mathbf{q} and branch index ν . Since the Fermi surface consists of multiple small sheets, a limited set of phonon wave vectors connect electronic states at the Fermi level. For example, $\mathbf{q} = \mathbf{K}$ (and nearby wave vectors) allows transitions between the two K-centered Fermi sheets, as shown in Fig. 2(b). Electron-phonon matrix elements were calculated for phonon wave vectors $\mathbf{q} = \Gamma, \mathbf{K}, \mathbf{M}$, and $\frac{1}{2}\Gamma\mathbf{K}$. For each of these wave vectors, we also sampled a few nearby points to estimate the phase-space weight $w_{\mathbf{q}}$, corresponding to a fraction of the area of the Brillouin zone, to assign each of the representative wave vectors. The dimensionless electron-phonon coupling parameter is then given by $\lambda = \sum_{\mathbf{q}\nu} 2N(0) \langle\langle |g_{\mathbf{q}\nu}|^2 \rangle\rangle w_{\mathbf{q}} / \hbar\omega_{\mathbf{q}\nu}$.

In Fig. 4, the total λ and the contributions from each representative phonon wave vector are plotted as a function of carrier concentration. For $x \lesssim 0.03$ electrons/f.u., the total coupling parameter λ is very small and only includes contributions from $\mathbf{q} = \Gamma$ (intrasheet) and \mathbf{K} (intersheet). The A_{1g} mode at the zone center has a large average electron-phonon matrix element, as previously

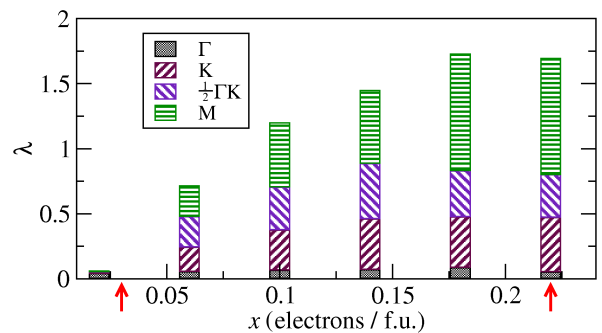


FIG. 4: (Color online) Electron-phonon coupling parameter calculated as a function of electron doping for single-layer MoS₂. Contributions from different phonon wave vectors are indicated by the shading. Arrows on the horizontal axis show where Fermi sheets appear or disappear.

noted, but the Brillouin-zone weight of this contribution to λ is limited by the small size of the Fermi sheets. For intersheet coupling, the average matrix element is found to be small, as is the weight. So even though the A_{1g} frequency is noticeably softened by electron-phonon coupling, the overall coupling constant, λ , is small.

Once the Fermi level reaches the Λ_{min} valley of the conduction band (or within a phonon energy of it), the coupling parameter acquires new contributions involving the Mo d_{xy/x^2-y^2} -like electronic states near Λ_{min} . The contributions to λ from phonon wave vectors $\mathbf{q} = \mathbf{K}$ and $\frac{1}{2}\Gamma\mathbf{K}$ are dominated by transitions from electronic states on one Λ_{min} Fermi sheet to another through absorption/emission of longitudinal acoustic phonons. In contrast, the longitudinal acoustic mode at $\mathbf{q} = \mathbf{M}$ strongly couples electronic states near Λ_{min} with those near \mathbf{K} . At the doping level of $x = 0.06$ electrons/f.u., taking into account the Brillouin-zone weights, each of the three phonon wave vectors that give rise to intersheet coupling have similar contributions to the total λ . As the carrier concentration is further increased, the coupling constant grows due to both matrix-element and phase-space factors. Above about $x = 0.18$ electrons/f.u., however, λ starts to decrease. This is mainly due to the shrinking of the Fermi sheets near \mathbf{K} , which are important for processes involving $\mathbf{q} = \mathbf{M}$ phonons.

To estimate the superconducting transition temperature, we used the Allen-Dynes formula³⁴ with $\mu^* = 0.13$. At low doping, before the Λ_{min} valley is occupied, T_c is calculated to be close to zero. Following the behavior of λ , T_c increases rapidly when the Λ_{min} Fermi sheets appear and grow, peaking near $x = 0.18$ electrons/f.u., with $T_c \approx 27$ K. It then decreases as the K-centered Fermi sheets shrink. Although the maximum λ of about 1.7 is larger than the value calculated for hole-doped graphane,³⁵ which has been predicted to be superconducting at liquid nitrogen temperatures, the T_c estimates for electron-doped single-layer MoS₂ are significantly lower because, unlike in graphane, where high-frequency C-C stretching modes dominate the cou-

pling, it is the acoustic modes that contribute most to the electron-phonon coupling in single-layer MoS₂. At $x = 0.18$ electrons/f.u., for example, the logarithmic average phonon frequency that sets the scale for T_c is about 160 cm^{-1} .

Because the K- and Λ_{min} -centered Fermi sheets have very different electronic character, interband anisotropy could enhance T_c in the doping regime when both valleys are occupied.³⁶ Using a two-band model,³⁷ we estimate that the effective coupling constant for superconductivity at $x = 0.18$ electrons/f.u. would increase to about 2.3. On the other hand, a BCS-like mean field treatment neglects phase fluctuations, which can renormalize T_c in 2D systems.³⁸ Since there are considerable uncertainties in the calculated transition temperatures, we focus instead on the trends, which should be robust.

The trends predicted for doping-induced superconductivity in single-layer MoS₂ are remarkably similar to the superconducting dome reported for electrostatically-doped thin flakes of MoS₂.¹⁹ However, it is not obvious that our monolayer results should match the experimental data for thin flakes. Even if the doping caused by gate tuning is limited to the first layer, the order of valleys in the conduction band is sensitive to interlayer interactions. In addition, our calculation does not take into account the effect of external electric fields on the electronic structure. Thus the order in which various Fermi sheets appear/disappear may be different in the thin-flake FET devices as compared to the single-layer system we investigated. Nevertheless, it seems likely that the features observed in the experiments, such as the onset of superconductivity at a critical carrier concentration, and the subsequent decrease in T_c at larger x , are associated with changes in the number and type of Fermi sheets as the gate is tuned.

To optimize electron-phonon coupling in electron-doped single-layer MoS₂, our work suggests that it is important to have carriers in both the K valley and Λ_{min} valley of the conduction band. This can be achieved over a very limited range of electrostatic doping. Since intercalated bulk MoS₂ exhibits superconductivity, chemical doping of single-layer MoS₂ may be an alternative route to superconductivity. As an example, we have investigated single-layer $K_x\text{MoS}_2$, where potassium adatoms are dispersed on one side of the MoS₂ layer. Supercells were used to examine three doping levels: $x = 0.11$, 0.25, and 0.33. At low doping, the potassium $4s$ band lies well above the bottom of the lowest MoS₂ conduction band, so the dopant simply transfers electrons into the MoS₂ conduction band. However, as the doping increases, the formation of a dipole layer at the interface causes the substrate bands to shift up in energy relative to the potassium s band. For $x = 0.25$, the bottom of the potassium s band lies slightly lower than the MoS₂ conduction band edge, though the two bands overlap in energy. At $x = 0.33$, the s band is split off and lies in the gap of the substrate band structure. For $K_{0.33}\text{MoS}_2$, we find $\lambda \sim 0.6$, indicating that the potassium $4s$ band couples

much more weakly to phonons than the MoS₂ conduction band. This highlights the importance of optimizing the character of electronic states at the Fermi level to enhance T_c , and demonstrates that different methods of doping (chemical vs. electrostatic) may lead to very different results. In neither case is a rigid band model adequate.

In summary, we find that the electron-phonon interaction in electron-doped MoS₂ depends sensitively on which valleys of the conduction band are occupied, since the orbital character of electronic states differ substantially in the different valleys. When both the K and Λ_{min} valleys are occupied, the electron-phonon coupling parameter is significant and suggests a superconducting T_c on the order of 20 K. The predicted trends in T_c , such as rapid changes when sheets of the Fermi surface appear and grow (or shrink and disappear), are similar to what has been observed in field-induced superconducting thin flakes of MoS₂,¹⁹ but further work is needed to bring the experimental and theoretical systems into closer contact. Given the difference in character between low-lying states in the conduction band and the importance of having the right mix of states at the Fermi level, mechanical or chemical tuning of the electronic structure could be promising routes for further enhancing the electron-phonon interaction in single-layer MoS₂ and related materials.

Acknowledgments

We thank P. Barbara and M. Calandra for helpful discussions. This work was supported by NSF Grant No. DMR-1006605.

-
- ¹ J. A. Wilson and A. D. Yoffe, *Adv. Phys.* **18**, 193 (1969).
- ² K. K. Kam and B. A. Parkinson, *J. Phys. Chem.* **86**, 463 (1982).
- ³ W. O. Winer, *Wear* **10**, 422 (1967).
- ⁴ W. K. Ho, J. C. Yu, J. Lin, J. G. Yu, P. S. Li, *Langmuir* **20**, 5865 (2004).
- ⁵ D. S. Thakur, B. Delmon, *J. Catal.* **91**, 308 (1985).
- ⁶ E. Gourmelon, O. Lignier, H. Hadouda, G. Couturier, J. C. Bernede, J. Tedd, J. Pouzet, and J. Salardenne, *Solar Energy Mater. Sol. Cells* **46**, 115 (1997).
- ⁷ See, for example, *Photoelectrochemistry and Photovoltaics of Layered Semiconductors*, ed. by A. Aruchamy (Kluwer, Dordrecht, 1992).
- ⁸ J. A. Woollam and R. B. Somoano, *Mater. Sci. Eng.* **31**, 289 (1977).
- ⁹ J. A. Woollam and R. B. Somoano, *Phys. Rev. B* **13**, 3843 (1976).
- ¹⁰ K. S. Novoselov, D. Jiang, F. Schedin, T. J. Booth, V. V. Khotkevich, S. V. Morozov, and A. K. Geim, *Proc. Natl. Acad. Sci. U.S.A.* **102**, 10451 (2005).
- ¹¹ D. Kim, D. Sun, W. Lu, Z. Cheng, Y. Zhu, D. Le, T. S. Rahman, and L. Bartels, *Langmuir* **27**, 11650 (2011).
- ¹² K. F. Mak, C. Lee, J. Hone, J. Shan, and T. F. Heinz, *Phys. Rev. Lett.* **105**, 136805 (2010).
- ¹³ A. Splendiani, L. Sun, Y. Zhang, T. Li, J. Kim, C.-Y. Chim, G. Galli, and F. Wang, *Nano Lett.* **10**, 1271 (2010).
- ¹⁴ A. Kuc, N. Zibouche, and T. Heine, *Phys. Rev. B* **83**, 245213 (2011).
- ¹⁵ B. Radisavljevic, A. Radenovic, J. Brivio, V. Giacometti, and A. Kis, *Nat. Nanotechnol.* **6**, 147 (2011).
- ¹⁶ F. K. Perkins, A. L. Friedman, E. Cobas, P. M. Campbell, G. G. Jernigan, and B. T. Jonker, *Nano Lett.* **13**, 668 (2013).
- ¹⁷ M. Fontana, T. Deppe, A. K. Boyd, M. Rinzan, A. Y. Liu, M. Paranjape, and P. Barbara, *Sci. Rep.* **3** 1634 (2013).
- ¹⁸ B. Chakraborty, A. Bera, D.V.S. Muthu, S. Bhowmick, U.V. Waghmare, and A.K. Sood, *Phys. Rev. B* **85**, 161403(R), (2012).
- ¹⁹ J. T. Ye, Y. J. Zhang, R. Akashi, M. S. Bahramy, R. Arita and Y. Iwasa, *Science* **30**, 1193 (2012).
- ²⁰ <http://www.quantumespresso.org>
- ²¹ D. Vanderbilt, *Phys. Rev. B* **41**, 7892 (1990).
- ²² J. P. Perdew and A. Zunger, *Phys. Rev. B* **23**, 5048 (1981).
- ²³ S. Baroni, S. de Gironcoli, A. Dal Corso and P. Giannozzi, *Rev. Mod. Phys.* **73**, 515 (2001).
- ²⁴ C. Ataca, M. Topsakal, E. Akturk, and S. Ciraci, *J. Phys. Chem. C* **115**, 16354 (2011).
- ²⁵ S. Lebegue and O. Eriksson, *Phys. Rev. B* **79**, 115409 (2009).
- ²⁶ K. Kaasbjerg, K. S. Thygesen, and K. W. Jacobsen, *Phys. Rev. B* **85**, 115317 (2012).
- ²⁷ H. Shi, H. Pan, Y. W. Zhang, and B. I. Yakobson, *Phys. Rev. B* **87**, 155304 (2013)
- ²⁸ Z. Y. Zhu, Y. C. Cheng, and U. Schwingenschlögl, *Phys. Rev. B* **84**, 153402 (2011).
- ²⁹ T. Cheiwchanchamnangij and W.R.L. Lambrecht, *Phys. Rev. B* **85**, 205302 (2012)
- ³⁰ A. Ramasubramaniam, *Phys. Rev. B* **86**, 115409 (2012).
- ³¹ C. Lee, H. Yan, L. E. Brus, T. F. Heinz, J. Hone, and S. Ryu, *ACS Nano* **4**, 2695 (2010).
- ³² H. S. S. Ramakrishna Matte, A. Giomathi, A. K. Manna, D. J. Late, R. Datta, S. K. Pati, and C. N. R. Rao, *Angew. Chem. Int. Ed.* **49**, 4059 (2010).
- ³³ A. Molina-Sanchez and L. Wirtz, *Phys. Rev. B* **84**, 155413 (2011).
- ³⁴ P. B. Allen and R. C. Dynes, *Phys. Rev. B* **12**, 905 (1975).
- ³⁵ G. Savini, A. C. Ferrari, and F. Giustino, *Phys. Rev. Lett.* **105**, 037002 (2010).
- ³⁶ H. Suhl, B. T. Matthias, and L. R. Walker, *Phys. Rev. Lett.* **3**, 552 (1959).
- ³⁷ A. Y. Liu, I. I. Mazin, and J. Kortus, *Phys. Rev. Lett.* **87**, 087005 (2001).
- ³⁸ W. Skocpol and M. Tinkham, *Rep. Prog. Phys.* **38**, 1049 (1975).